Elastic-plastic solutions for expanding cavities embedded in two different cohesive-frictional materials

Pin-Qiang Mo, Alec M. Marshall[*,†] and Hai-Sui Yu

Faculty of Engineering, University of Nottingham, University Park, Nottingham NG7 2RD, U.K.

SUMMARY

An analytical solution of cavity expansion in two different concentric regions of soil is developed and investigated in this paper. The cavity is embedded within a soil with finite radial dimension and surrounded by a second soil, which extends to infinity. Large-strain quasi-static expansion of both spherical and cylindrical cavities in elastic-plastic soils is considered. A non-associated Mohr–Coulomb yield criterion is used for both soils. Closed-form solutions are derived, which provide the stress and strain fields during the expansion of the cavity from an initial to a final radius. The analytical solution is validated against finite element simulations, and the effect of varying geometric and material parameters is studied. The influence of the two different soils during cavity expansion is discussed by using pressure–expansion curves and by studying the development of plastic regions within the soils. The analytical method may be applied to various geotechnical problems, which involve aspects of soil layering, such as cone penetration test interpretation, ground-freezing around shafts, tunnelling, and mining. © 2014 The Authors. *International Journal for Numerical and Analytical Methods in Geomechanics* published by John Wiley & Sons Ltd.

1. INTRODUCTION

Cavity expansion theory has been extensively developed and widely used for the study of many engineering problems. Since its early application to geotechnical problems in the 1960s [1], many analytical solutions have been proposed using increasingly sophisticated constitutive soil models. Vesic [2] presented an approximate solution for spherical cavity expansion in an infinite soil mass using a compressible Mohr–Coulomb material. The analysis was applied to evaluate the bearing capacity factors of deep foundations. Carter *et al.* [3] derived closed-form solutions for cavity expansion from zero initial radius in an ideal cohesive-frictional material with a small-strain restriction. The deformations in the elastic region were assumed to be infinitesimal, and the convected term of the stress rate was neglected in the governing equation, which provided an approximate limit pressure solution. Yu and Houlsby [4] provided a unified analytical solution of cavity expansion in dilatant elastic-plastic soils, using the Mohr–Coulomb yield criterion with a non-associated flow rule. The complete large-strain analysis, with the aid of a series expansion, was introduced to derive a rigorous closed-form solution without any additional restrictions or assumptions. The limitation of their analysis was that the material properties were assumed to be constant and independent of stress–strain history. Salgado *et al.* [5] reported a cylindrical cavity expansion solution and produced a stress rotation analysis for the

interpretation of the cone penetration test (CPT). A numerical formulation was used in the plastic region to achieve a variable stiffness, friction angle, and dilation angle.

As reviewed by Yu [6], the cavity expansion theory has mainly been applied in the geotechnical engineering areas of in-situ soil testing [5, 7–11], deep foundations [12–15], tunnels and underground excavations [16–18], and recently, for an interaction analysis between tunnels and piles [19, 20]. Despite the wide application of the theory to geotechnical problems, very little work has been carried out to consider the effect of distinct soil regions within the framework of cavity expansion analyses. The work of Xu and Lehane [21] is notable for its use of a numerical analysis of spherical cavity expansion for investigating pile or probe resistance in two-layered soil profiles.

Analytical cavity expansion solutions for two concentrically layered media were developed by Bernard [22, 23] for the study of projectile penetration. The analysis considered an incompressible material as well as the assumption of a finite locking strain and was used to solve for dynamic solutions of penetration depth and impact velocity. Sayed and Hamed [24] were the first to apply analytical cavity expansion analyses of concentrically layered media to the field of geomechanics. However, in their analysis, the medium was assumed to be a frictionless linear-elastic solid and did not account for the plastic behaviour of soils. In this paper, the analytical solution described by Yu and Houlsby [4] is extended in order to consider a cavity embedded within a profile of two different concentric regions of soil. The soil is treated as an isotropic dilatant elastic-perfectly plastic material with a Mohr–Coulomb yield criterion and a non-associated flow rule. Large-strain quasi-static expansion of both spherical and cylindrical cavities is considered. The complete large-strain expansion for non-associated Mohr–Coulomb materials in two concentric media has not previously been presented in the literature. The development of an analytical cavity expansion method for application to geotechnical problems involving aspects of soil layering is the main motivation for the work described in this paper. The focus here is on the development of the analytical method; its application to practical geotechnical problems will be explored in future publications.

The paper begins with a general definition of the problem and the necessary geometric parameters. The following section considers the most general expansion problem for a cavity embedded in two different concentric regions of soil and derives expressions for stresses, strains, and displacements within elastic and plastic zones. The cavity expansion solution is then validated against results obtained using the Finite Element (FE) method. Further results and parametric analyses are then presented with focus placed on the resulting pressure–expansion curves and the development of plastic regions within the two soil zones. A discussion of the application of the proposed method and its limitations is provided, followed by concluding remarks.

2. DEFINITION OF PROBLEM

The problem involves three concentric zones; (i) an inner zone representing the expanding cavity, (ii) a second zone representing Soil A, and (iii) a bounding region, which extends to infinity and represents Soil B, as shown in Figure 1(a). Initially, the cavity has a radius a_0, and the interface between Soils A and B is located at a radial distance b_0 from the centre of the cavity. The soils are assumed to be isotropic homogeneous media; therefore, an initial hydrostatic stress P_0 acts throughout both Soils A and B as well as within the cavity. Note that a tension positive notation is used in this paper.

When the cavity pressure P_a increases slowly from its initial value P_0, the radius of cavity and Soil A/B interface are expanded to a and b, respectively (Figure 1(b)). The pressure at the Soil A/B interface is given by P_b. Depending on material properties (and adopting the Mohr–Coulomb yield criterion), a plastic region may form within either of the Soils A or B and extend to some radial distance c_A or c_B, respectively. For a given increment of cavity expansion, the initial plastic-elastic interfaces in Soils A and B are given by c_{0A} and c_{0B}, respectively. The radial stresses at the plastic-elastic interfaces for Soils A and B are defined as P_{c_A} and P_{c_B}, respectively.

As in the work of Yu and Houlsby [4], the soils are modelled as an isotropic dilatant elastic-perfectly plastic material, obeying Hooke's law for elastic analysis and the Mohr–Coulomb yield criterion with a non-associated flow rule for plastic analysis. The properties of Soils A and B are denoted by subscripts 1 and 2, respectively: Young's modulus (E_1, E_2), Poisson's ratio (ν_1, ν_2), cohesion (C_1, C_2), friction angle (ϕ_1, ϕ_2), and dilation angle (ψ_1, ψ_2).
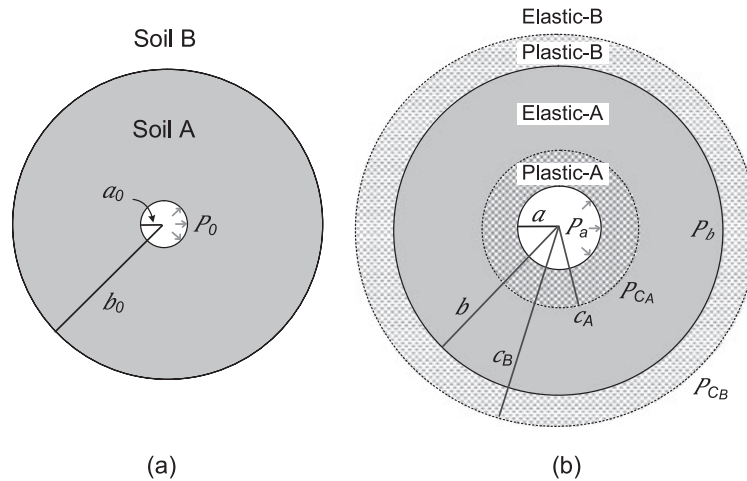
Figure 1. Schematic view of the model of cavity expansion in two concentric regions of soil.
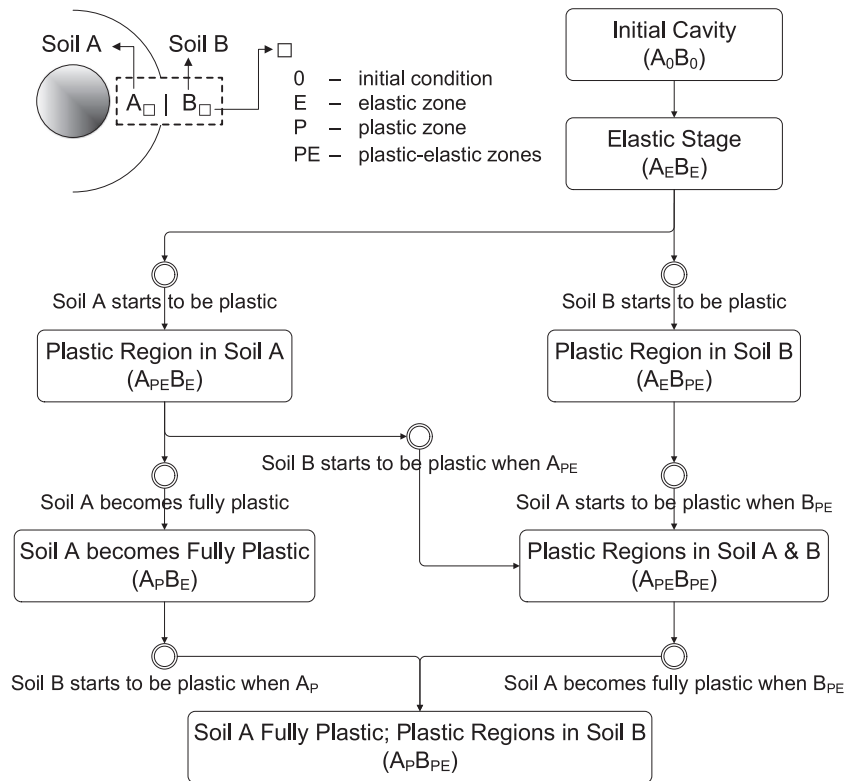

Figure 2. Flow chart of cavity expansion in two concentric regions of soil.

To combine both spherical and cylindrical analyses, the parameter k is used to indicate spherical analysis ($k = 2$) or cylindrical analysis ($k = 1$). It should be noted that for the cylindrical case, plane strain conditions in the z direction are assumed and the axial stress is assumed as the intermediate principal stress, which is satisfied for most realistic values of soil parameters, as discussed by Yu and Houlsby [4]. In accordance with Yu [6], the following parameters are used for mathematical convenience (definitions provided in the Appendix): $G, M, Y, \alpha, \beta, \gamma, \delta$.

During cavity expansion, plastic regions in the two concentric soils are generated and develop depending on the relevant properties and profiles of Soils A and B. Considering all possible situations, the expansion process would follow one of the routes in the flow chart illustrated in Figure 2, which

also provides a definition of some notation. Generally, during expansion of the cavity from a_0 to a, an elastic stage ($A_E B_E$) appears initially, followed by plastic regions developing in both Soils A and B as a increases ($A_{PE} B_{PE}$). Ultimately, as a is increased further, Soil A becomes fully plastic ($A_P B_{PE}$) (Soil B extends to infinity and therefore never becomes fully plastic). The events at the circular nodes in the flow chart describe the situation of expansion and determine the appropriate state of soil to be considered. The solutions provided here are for the most general case of expansion ($A_{PE} B_{PE}$); all the scenarios described in Figure 2 can be deduced from this general solution.

3. CAVITY EXPANSION IN TWO CONCENTRIC REGIONS OF SOIL

3.1. Solution in elastic regions

As illustrated in Figure 1, for an arbitrary radial distance r, the material is elastic in the zones where $r > c_B$ (Soil B) and where $c_A < r < b$ (Soil A). Under conditions of radial symmetry, the stresses within the soils around the cavity must satisfy the following equation of equilibrium:

$$\sigma_\theta - \sigma_r = \frac{r}{k} \frac{\partial \sigma_r}{\partial r} \tag{1}$$

where σ_r and σ_θ are stresses acting in the radial and tangential directions, respectively; the parameter $k = 1$ is for cylindrical symmetry and $k = 2$ is for spherical symmetry.

Correspondingly, the radial and tangential strain for small-strain analysis in the elastic regions can be expressed as a function of the radial displacement u:

$$\epsilon_r = \frac{d u}{d r} \quad ; \quad \epsilon_\theta = \frac{u}{r} \tag{2}$$

For the elastic region in Soil A ($c_A < r < b$), with Hooke's law, the solutions for the radial displacement and stresses are expressed as

$$u = D_1 r + \frac{D_2}{r^k} \tag{3}$$

$$
\sigma_r = \frac{M_1}{-k \left[\frac{v_1}{1 - v_1 (2-k)} \right]^2 + [1 - v_1 (k-1)]}
$$
$$
\times \left\{ [1 - v_1 (k-1)] \left(D_1 - k \frac{D_2}{r^{k+1}} \right) + k \frac{v_1}{1 - v_1 (2-k)} \left(D_1 + \frac{D_2}{r^{k+1}} \right) \right\} - P_0 \tag{4}
$$

$$
\sigma_\theta = \frac{M_1}{-k \left[\frac{v_1}{1 - v_1 (2-k)} \right]^2 + [1 - v_1 (k-1)]}
$$
$$
\times \left[\frac{v_1}{1 - v_1 (2-k)} \left(D_1 - k \frac{D_2}{r^{k+1}} \right) + \left(D_1 + \frac{D_2}{r^{k+1}} \right) \right] - P_0 \tag{5}
$$

where D_1 and D_2 are integration constants defined as

$$D_1 = \frac{(c_A - c_{0A}) c_A{}^k - (b - b_0) b^k}{c_A{}^{k+1} - b^{k+1}} \quad ; \quad D_2 = \frac{(c_{0A} b - c_A b_0) c_A{}^k b^k}{c_A{}^{k+1} - b^{k+1}} \tag{6}$$

The solutions are subject to two stress boundary conditions:

$$\sigma_r|_{r=c_A} = -P_{c_A} \quad ; \quad \sigma_r|_{r=b} = -P_b \tag{7}$$

Similarly, the following solutions for the radial displacement and stress in Soil B ($r > c_B$) are obtained:

$$u = c_B{}^k (c_B - c_{0B}) \frac{1}{r^k} \tag{8}$$

$$\sigma_r = \frac{M_2}{-k\left[\frac{v_2}{1-v_2(2-k)}\right]^2 + [1-v_2(k-1)]}$$
$$\times \left\{ k\left[\frac{v_2}{1-v_2(2-k)} - [1-v_2(k-1)]\right] \frac{c_B{}^k (c_B - c_{0B})}{r^{k+1}} \right\} - P_0 \tag{9}$$

$$\sigma_\theta = \frac{M_2}{-k\left[\frac{v_2}{1-v_2(2-k)}\right]^2 + [1-v_2(k-1)]} \left[\left(1 - k\frac{v_2}{1-v_2(2-k)}\right) \frac{c_B{}^k (c_B - c_{0B})}{r^{k+1}}\right] - P_0 \tag{10}$$

which is subject to the stress boundary condition:

$$\sigma_r|_{r=c_B} = -P_{c_B} \tag{11}$$

3.2. Solution in plastic region of Soil A: ($a < r < c_A$)

In order to account for the effect of large strain in the plastic regions, logarithmic strains are adopted, namely

$$\epsilon_r = \ln\left(\frac{d\,r}{d\,r_0}\right) \quad ; \quad \epsilon_\theta = \ln\left(\frac{r}{r_0}\right) \tag{12}$$

Using the tension positive notation, the Mohr–Coulomb yield condition in Soil A during cavity expansion is

$$\alpha_1 \sigma_\theta - \sigma_r = Y_1 \tag{13}$$

where α_1 and Y_1 are functions related to friction angle and cohesion (Appendix). It may be noted that when the friction angle is zero, the Mohr–Coulomb yield function reduces to the Tresca criterion.

The stress components in the plastic region of Soil A must satisfy equilibrium (equation 1) and the yield condition (equation 13) as follows:

$$\sigma_r = \frac{Y_1}{\alpha_1 - 1} + A_1 r^{-\frac{k(\alpha_1 - 1)}{\alpha_1}} \quad ; \quad \sigma_\theta = \frac{Y_1}{\alpha_1 - 1} + \frac{A_1}{\alpha_1} r^{-\frac{k(\alpha_1 - 1)}{\alpha_1}} \tag{14}$$

where A_1 is a constant of integration and where σ_r has two stress boundary conditions:

$$\sigma_r|_{r=c_A} = -P_{c_A} \quad ; \quad \sigma_r|_{r=a} = -P_a \tag{15}$$

Combining the expressions in equation (15) leads to

$$\frac{P_a + \frac{Y_1}{\alpha_1 - 1}}{P_{c_A} + \frac{Y_1}{\alpha_1 - 1}} = \left(\frac{c_A}{a}\right)^{\frac{k(\alpha_1 - 1)}{\alpha_1}} \tag{16}$$

$$A_1 = -\left(P_a + \frac{Y_1}{\alpha_1 - 1}\right) a^{\frac{k(\alpha_1 - 1)}{\alpha_1}} = -\left(P_{c_A} + \frac{Y_1}{\alpha_1 - 1}\right) c_A^{\frac{k(\alpha_1 - 1)}{\alpha_1}} \tag{17}$$

For the displacement analysis in the plastic region, total strain is considered as the sum of elastic and plastic contributions, using superscripts e and p, respectively. Elastic strain (equivalent to strain rate $\dot{\epsilon}$ for this case because initial strains are zero) can be derived from equations (4) and (5):

$$\dot{\epsilon}_r{}^e = \frac{1}{M_1}\left[\dot{\sigma}_r - \frac{k\,v_1}{1-v_1(2-k)}\dot{\sigma}_\theta\right] \tag{18}$$

$$\dot{\epsilon}_\theta{}^e = \frac{1}{M_1}\left\{-\frac{v_1}{1-v_1(2-k)}\dot{\sigma}_r + [1-v_1(k-1)]\dot{\sigma}_\theta\right\} \tag{19}$$

where $\dot{(\,)}$ is the corresponding incremental form.

The non-associated Mohr–Coulomb flow rule for loading phase in Soil A can be expressed as

$$\frac{\dot{\epsilon}_r{}^p}{\dot{\epsilon}_\theta{}^p} = \frac{\dot{\epsilon}_r - \dot{\epsilon}_r{}^e}{\dot{\epsilon}_\theta - \dot{\epsilon}_\theta{}^e} = -\frac{k}{\beta_1} \tag{20}$$

where β_1 is a function of dilation angle. If $\beta_1 = \alpha_1$ (dilation angle = friction angle), then the flow rule for Soil A is said to be fully associated. This plastic-flow rule was proposed by Davis [25], assuming that the soil dilates plastically at a constant rate.

Substituting elastic strain equations (18) and (19) into the plastic-flow rule equation (20) results in

$$\beta_1 \dot{\epsilon}_r + k \dot{\epsilon}_\theta = \frac{1}{M_1}\left[\beta_1 - \frac{k\,\nu_1}{1 - \nu_1\,(2-k)}\right]\dot{\sigma}_r$$
$$+ \frac{1}{M_1}\left[k\,(1-2\,\nu_1) + 2\,\nu_1 - \frac{k\,\nu_1\,\beta_1}{1 - \nu_1\,(2-k)}\right]\dot{\sigma}_\theta \tag{21}$$

With logarithmic strain equations (12), substituting equations (14) and applying the initial stress conditions into equation (21) leads to

$$\ln\left[\left(\frac{r}{r_0}\right)^{\frac{k}{\beta_1}} \cdot \frac{d\,r}{d\,r_0}\right] = \ln \chi_1 + \mu_1 A_1 \left(\frac{1}{r}\right)^{\frac{k\,(\alpha_1-1)}{\alpha_1}} \tag{22}$$

where

$$\chi_1 = exp\left\{\frac{(\beta_1 + k)\,(1-2\,\nu_1)\,[1 + (2-k)\,\nu_1]\,[Y_1 + (\alpha_1 - 1)\,P_0]}{E_1\,(\alpha_1 - 1)\,\beta_1}\right\} \tag{23}$$

$$\mu_1 = \frac{1 + \nu_1\,(2-k)}{E_1\,\alpha_1\,\beta_1}\{[\beta_1 + (k-2)\,\nu_1\,\beta_1 - k\,\nu_1]\,\alpha_1 + k\,(1 - \nu_1 - \nu_1\,\beta_1)\} \tag{24}$$

By means of transformation $\varrho = -A_1 \left(\frac{1}{r}\right)^{\frac{k\,(\alpha_1-1)}{\alpha_1}}$, equation (22) can be integrated over the interval $[\,c_A, r\,]$, leading to

$$\frac{\chi_1}{\gamma_1} \cdot (-A_1)^{-\gamma_1} \cdot \left(c_{0A}{}^{\frac{\beta_1+k}{\beta_1}} - r_0{}^{\frac{\beta_1+k}{\beta_1}}\right) = \int_{P_{c_A}+\frac{Y_1}{\alpha_1-1}}^{\varrho} e^{\mu_1 \varrho} \cdot \varrho^{-1-\gamma_1}\,d\varrho \tag{25}$$

By putting $r = a$, $r_0 = a_0$ and $\varrho\,|_{r=a} = P_a + \frac{Y_1}{\alpha_1-1}$, we find

$$\frac{\chi_1}{\gamma_1}\left(P_a + \frac{Y_1}{\alpha_1 - 1}\right)^{-\gamma_1} \cdot \left[\left(\frac{c_{0A}}{a}\right)^{\frac{\beta_1+k}{\beta_1}} - \left(\frac{a_0}{a}\right)^{\frac{\beta_1+k}{\beta_1}}\right] = \int_{P_{c_A}+\frac{Y_1}{\alpha_1-1}}^{P_a+\frac{Y_1}{\alpha_1-1}} e^{\mu_1 \varrho} \cdot \varrho^{-1-\gamma_1}\,d\varrho \tag{26}$$

With the aid of the series expansion

$$e^{\mu_1 \varrho} = \sum_{n=0}^{\infty} \frac{(\mu_1\,\varrho)^n}{n!} \tag{27}$$

equation (26) is found to be

$$\frac{\chi_1}{\gamma_1}\left(P_a + \frac{Y_1}{\alpha_1 - 1}\right)^{-\gamma_1} \cdot \left[\left(\frac{c_{0A}}{a}\right)^{\frac{\beta_1+k}{\beta_1}} - \left(\frac{a_0}{a}\right)^{\frac{\beta_1+k}{\beta_1}}\right]$$
$$= \sum_{n=0}^{\infty} \begin{cases} \frac{\mu_1{}^n}{n!}\,\ln\left[\frac{P_a+\frac{Y_1}{\alpha_1-1}}{P_{c_A}+\frac{Y_1}{\alpha_1-1}}\right] & \text{if } n = \gamma_1 \\ \frac{\mu_1{}^n}{n!\,(n-\gamma_1)}\left[\left(P_a + \frac{Y_1}{\alpha_1-1}\right)^{n-\gamma_1} - \left(P_{c_A} + \frac{Y_1}{\alpha_1-1}\right)^{n-\gamma_1}\right] & \text{otherwise} \end{cases} \tag{28}$$

To calculate the distribution of displacements within the plastic region of Soil A, without imposing any boundary conditions, equation (25) can be written as

$$\frac{\chi_1}{\gamma_1} \left(P_a + \frac{Y_1}{\alpha_1 - 1} \right)^{-\gamma_1} \cdot \left[\left(\frac{c_{0A}}{a} \right)^{\frac{\beta_1 + k}{\beta_1}} - \left(\frac{r_0}{a} \right)^{\frac{\beta_1 + k}{\beta_1}} \right] = \Lambda_1(r)$$

$$\Lambda_1(r) = \sum_{n=0}^{\infty} \begin{cases} \frac{\mu_1{}^n}{n!} \left[\ln \varrho - \ln \left(P_{c_A} + \frac{Y_1}{\alpha_1 - 1} \right) \right] & \text{if } n = \gamma_1 \\ \frac{\mu_1{}^n}{n! (n - \gamma_1)} \left[\varrho^{n - \gamma_1} - \left(P_{c_A} + \frac{Y_1}{\alpha_1 - 1} \right)^{n - \gamma_1} \right] & \text{otherwise} \end{cases} \tag{29}$$

Hence, displacement u is

$$u = r - r_0 = r - \left[-\Lambda_1(r) \cdot \frac{\gamma_1}{\chi_1} \cdot \left(P_a + \frac{Y_1}{\alpha_1 - 1} \right)^{\gamma_1} + \left(\frac{c_{0A}}{a} \right)^{\frac{\beta_1 + k}{\beta_1}} \right]^{\frac{\beta_1}{\beta_1 + k}} \cdot a \tag{30}$$

To calculate the strain distribution, equation (30) can be rewritten in terms of $\frac{r}{r_0}$ and derived to give an equation in terms of $\frac{dr}{dr_0}$. The final strain distribution is then obtained using logarithmic strains for large-strain analysis.

3.3. Solution in plastic region of Soil B: ($b < r < c_B$)

Similarly, by using the corresponding equilibrium equation and yield condition, the stress components in the plastic region of Soil B are shown to be in the form

$$\sigma_r = \frac{Y_2}{\alpha_2 - 1} + A_2 \, r^{-\frac{k (\alpha_2 - 1)}{\alpha_2}} \qquad ; \qquad \sigma_\theta = \frac{Y_2}{\alpha_2 - 1} + \frac{A_2}{\alpha_2} r^{-\frac{k (\alpha_2 - 1)}{\alpha_2}} \tag{31}$$

where A_2 is a constant of integration and radial stress has two boundary conditions:

$$\sigma_r|_{r=c_B} = -P_{c_B} \qquad ; \qquad \sigma_r|_{r=b} = -P_b \tag{32}$$

From the stress in the elastic region in Soil B, we can find

$$\frac{c_B}{b} = \left\{ \frac{(k + \alpha_2) [Y_2 + (\alpha_2 - 1) P_b]}{(k + 1) \alpha_2 [Y_2 + (\alpha_2 - 1) P_0]} \right\}^{\frac{\alpha_2}{k (\alpha_2 - 1)}} = R_2^{\frac{\alpha_2}{k (\alpha_2 - 1)}} \tag{33}$$

where R_2 is a parameter, which is related to the pressure at the interface between Soils A and B (P_b). The solution for plastic displacements in Soil B can be obtained by the equations of Yu and Houlsby [4], which provides the following for the pressure–expansion relationship:

$$\left(\frac{b}{b_0} \right)^{\frac{\beta_2 + k}{\beta_2}} = \frac{R_2^{-\gamma_2}}{(1 - \delta_2)^{\frac{\beta_2 + k}{\beta_2}} - \frac{\gamma_2}{\chi_2} \Lambda_2(R_2, \mu_2)} \tag{34}$$

in which Λ_2 is defined by

$$\Lambda_2(R_2, \mu_2) = \sum_{n=0}^{\infty} \begin{cases} \frac{\mu_2{}^n}{n!} \ln R_2 & \text{if } n = \gamma_2 \\ \frac{\mu_2{}^n}{n! (n - \gamma_2)} [(R_2)^{n - \gamma_2} - 1] & \text{otherwise} \end{cases} \tag{35}$$

and

$$\chi_2 = \exp \left\{ \frac{(\beta_2 + k) (1 - 2 v_2) [1 + (2 - k) v_2] [Y_2 + (\alpha_2 - 1) P_0]}{E_2 (\alpha_2 - 1) \beta_2} \right\} \tag{36}$$

$$\mu_2 = \frac{(k + 1) \delta_2 [1 - v_2{}^2 (2 - k)]}{(1 + v_2) (\alpha_2 - 1) \beta_2} \left[\alpha_2 \beta_2 + k (1 - 2 v_2) + 2 v_2 - \frac{k v_2 (\alpha_2 + \beta_2)}{1 - v_2 (2 - k)} \right] \tag{37}$$

To calculate the distribution of displacements in the plastic region of Soil B, u can be written as the following equation, which in-turn can be used to derive the strain distribution:

$$u = r - r_0 = r - \left[-\int_1^\varrho e^{\mu_2 \varrho} \cdot \varrho^{-1-\gamma_2} \, d\varrho \cdot \frac{\gamma_2}{\chi_2} + (1-\delta_2)^{\frac{\beta_2+k}{\beta_2}} \right]^{\frac{\beta_2}{\beta_2+k}} \cdot c_B \qquad (38)$$

4. VALIDATION WITH FINITE ELEMENT SIMULATION

The accuracy of the analytical model was initially confirmed against results obtained with the fundamental solutions from Yu and Houlsby [4] for the case where the properties of Soils A and B were identical. To further validate the analytical model, two FE numerical models were developed in Abaqus/Standard and used to simulate the expansion of both spherical and cylindrical cavities, as shown in Figure 3. The axis-symmetric option was used in Abaqus in order to achieve spherical and cylindrical analyses using the 2D models. The cavity was expanded from an initial radius of 6 mm under an initial pressure of 1 kPa. The initial radius of the Soil A/B interface (given by b_0) was 30 mm, while Soil B had a radius D, which was large enough to make boundary effects negligible. In the numerical simulations, the properties of both Soils A and B were set as follows: $\nu = 0.2$, $\phi = 10°$, $\psi = 10°$, $C = 10$ kPa.

A total of four expansion tests were carried out using the numerical model in which the Young's modulus (E) of Soils A and B was either 1 or 10 MPa (results presented in Figure 4). The labels on the figure indicate the model (analytical = CEM; numerical = FEM), followed by the value of Young's modulus of Soil A and B, respectively. Hence, the label CEM-10-1 relates to the analytical cavity expansion analysis results in which Soil A has $E_1 = 10$ MPa and Soil B has $E_2 = 1$ MPa. Figure 4 shows that very good agreement between analytical and numerical results was obtained.

As indicated in Figure 4(a) for spherical expansion, for the uniform soil tests ('-10-10' and '-1-1'), the cavity pressure (P_a) increases gradually with cavity displacement and asymptotically approaches a limit pressure. The limit pressure of the soil with $E = 10$ MPa is shown to be nearly twice as large as that with $E = 1$ MPa. For the tests with two different soils (two-region tests), the pressure–expansion curves initially follow the trend in which the E of the uniform soil tests matches the value of E in Soil A of the two-region tests (i.e. '-10-1' matches '10-10' and '-1-10' matches '-1-1'). At a certain stage, the existence of Soil B begins to have an effect, and the pressure–expansion curve of the two-region

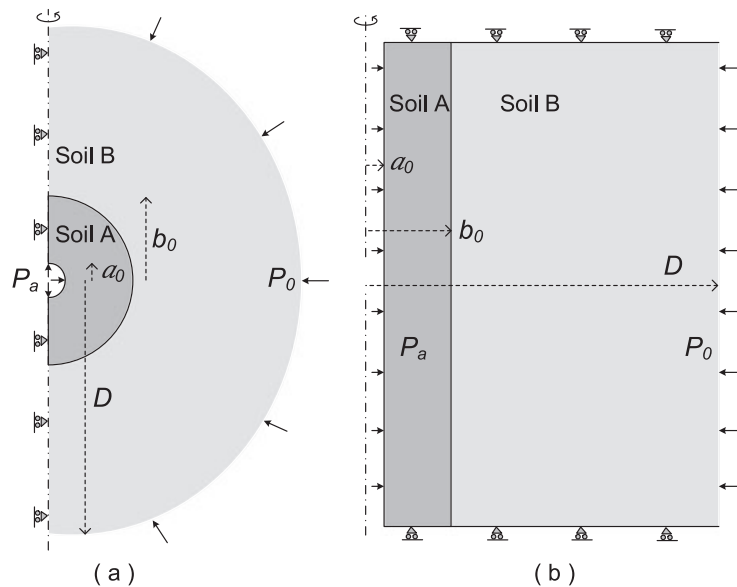(a)   (b)

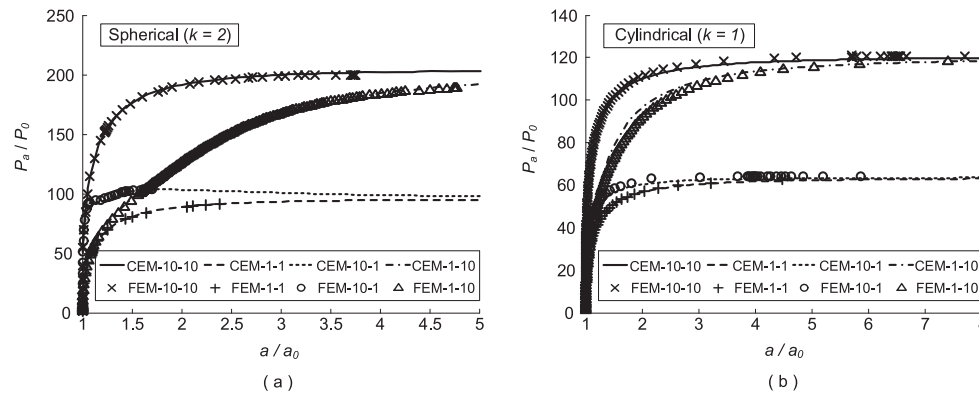Figure 3. Finite element models for (a) spherical cavity expansion; (b) cylindrical cavity expansion.

Figure 4. Comparison between numerical results and analytical solutions: (a) spherical cavity expansion; (b) cylindrical cavity expansion.

analysis tends towards the limit pressure obtained from the uniform soil test in which E matches that of Soil B of the two-region test (i.e. ultimately '-10-1' approaches '1-1' and '-1-10' approaches '-10-10'). Figure 4(b) shows equivalent results for cylindrical cavity expansion and illustrates that cylindrical pressures are about 60 % of those from the spherical analysis.

The effect of a distinct change in soil stiffness on the pressure expansion curves is shown to be significant in Figure 4. The limit pressure is often applied to investigate pile capacity or probe resistance in conventional cavity expansion solutions (e.g. [13]). This approach is appropriate for uniform soils because the limiting pressure is only affected by the parameters of a single soil. For concentric regions of two different soils, Figure 4 shows that the limiting pressure depends only on the properties of Soil B. For penetration problems such as CPT or pile capacity analysis, the resistance of a probe located in Soil A will certainly depend on the properties of Soil A, so the limit pressure approach may not be adequate for cases where two different soils affect results (e.g. layered soils). A more suitable approach for layered soils, as suggested by Xu and Lehane [21], is to consider a realistic increase in cavity size (given by $a/a0$) and to evaluate the cavity pressure required to achieve this expansion. The results of such an approach for the case of cavity expansion in two concentric regions of different soils (rather than horizontally layered soils) are explored further in the next section.

5. RESULTS

This section considers the cavity expansion method in two concentric regions of different soils and investigates the effect of various parameters on model results. Results are based on the expansion of a cavity from $a_0 = 0.1$ mm to $a = 6$ mm ($a/a_0 = 60$). As illustrated in Figure 4, the two-region tests are highly sensitive to the ratio a/a_0 (the value of a_0 has no effect on the normalised pressure expansion curves as long as the ratio of b_0/a_0 is maintained). The selection of these cavity parameters was based on geotechnical centrifuge experiments being carried out as part of this research (to be published in a future paper) in which a 6 mm radius penetrometer is pushed into sand with an average grain size of approximately 0.1 mm. The cavity expansion analysis was conducted with a Soil A/B interface at $b_0 = 30$ mm and initial hydrostatic stress $P_0 = 1$ kPa. The following material parameters are taken for baseline comparison (note that subscripts 1 and 2 refer to Soils A and B, respectively): $\nu_1 = \nu_2 = 0.2$; $\phi_1 = \phi_2 = 40°$; $\psi_1 = \psi_2 = 10°$; $C_1 = C_2 = 0$ kPa. As in the previous section, results here focus mainly on the effect of varying the value of Young's modulus E of the two soils ($E_1 = 10$ or 1 MPa; $E_2 = 10$ or 1 MPa).

Figure 5 shows the distribution of radial (a, b) and tangential (c, d) stresses respectively, for both spherical and cylindrical cavity expansion, as radial distance from the cavity (r) is increased. The results from the two-region tests are bounded by the results from the uniform soil tests ('-10-10' and '-1-1'). A sharper decrease in stresses is noted for the spherical cases compared to the cylindrical cases.
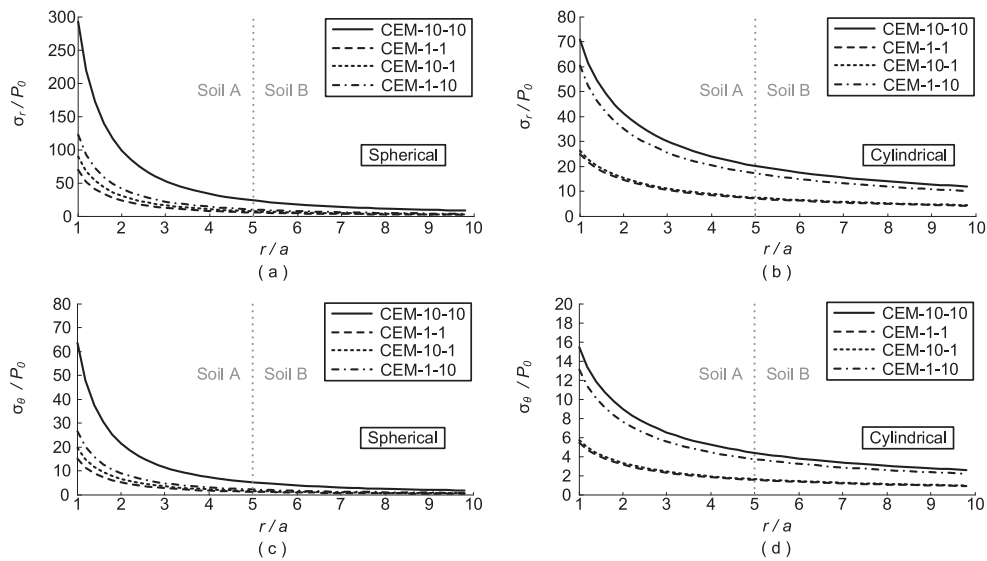
Figure 5. Radial (a, b) and tangential (c, d) stress distributions around cavity for both spherical and cylindrical cavity expansion (for $a/a_0 = 60$).
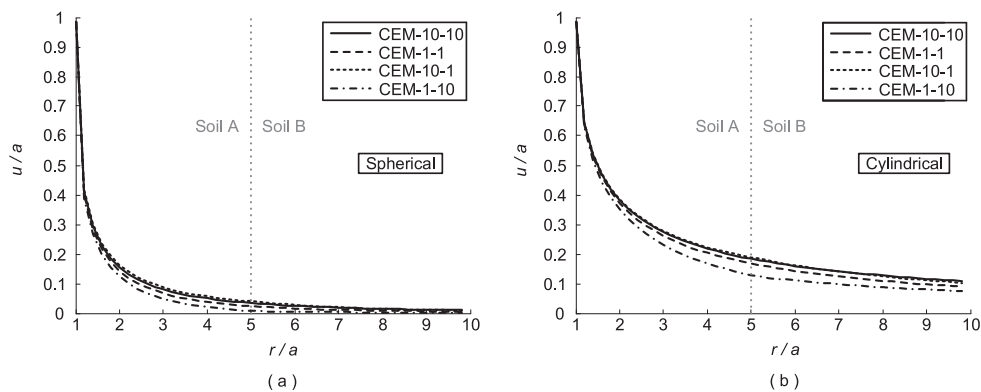

Figure 6. Displacement distribution around cavity: (a) spherical cavity expansion; (b) cylindrical cavity expansion (for $a/a_0 = 60$).

There is an interesting difference between the spherical and cylindrical analysis results. For the cylindrical tests, the results for the two-region analysis appear to be mainly controlled by the value of E of Soil B ('-10-1' effectively matches '-1-1' and '-1-10' is close to '-10-10'). For the spherical tests, however, the data from both the two-region tests are close to the uniform test '-1-1'. The reason for this behaviour is the different degree of interaction between Soils A and B within the spherical and cavity expansion analyses, which will be discussed later in the text using pressure–expansion curves (Figure 8).

Normalised displacement distributions are presented in Figure 6 and show that results for all tests closely agree. This is due to the kinematic nature of the expansion problem; the differences between the lines shown in Figure 6 (for constant values of friction and dilation angles in Soils A and B) are due only to the effect of yielding. For purely elastic behaviour, the displacements are insensitive to the elastic parameters (as in the elastic half-plane analysis of Verruijt and Booker [26] for displacements around tunnels).

The spherical test 'CEM-1-10' is selected to investigate the variation of displacement with strength and plastic-flow parameters (i.e. friction and dilation angles), as shown in Figure 7. For tests with uniform parameters in Soils A and B, the displacements increase with an increase in dilation angle
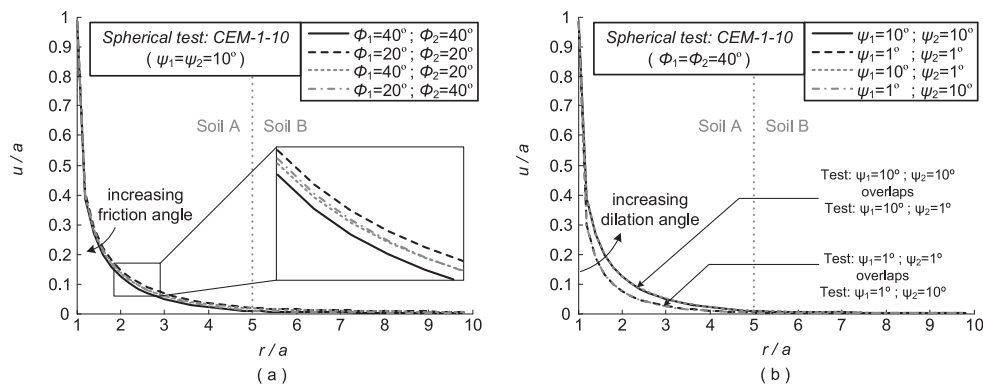
Figure 7. Variation of displacement distribution with (a) friction angle and (b) dilation angle for spherical test: CEM-1-10 (for $a/a_0 = 60$).
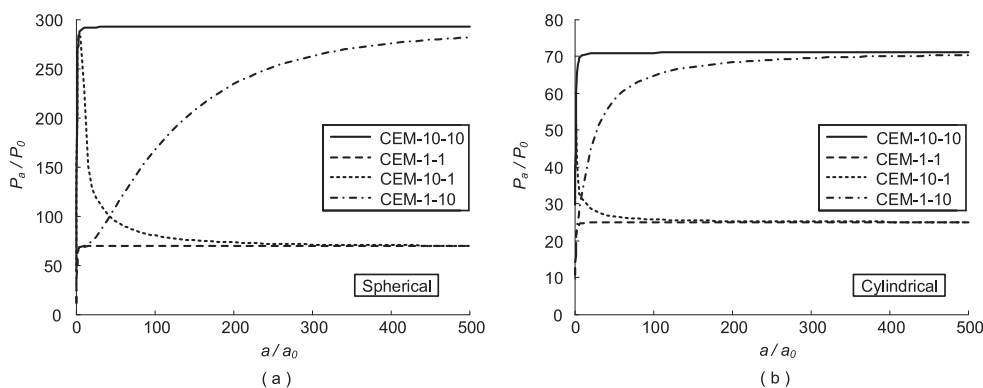

Figure 8. Variation of cavity pressure with cavity radius: (a) spherical cavity expansion; (b) cylindrical cavity expansion.

(Figure 7(b)), whereas displacements decrease only marginally with an increase in friction angle (Figure 7(a)). The effect of varying friction angle of the two soils in the two-region tests is difficult to observe because the overall effect on displacements is small. The magnified zone in Figure 7(a) shows that the effect of friction angle is bounded by the uniform tests. The magnitudes of the differences are of little practical concern. For dilation angle, the behaviour for the two-region tests is dominated by the value of dilation angle in Soil A, where the lines with equal values of ψ_1 are shown to overlap in Figure 7(b).

The pressure–expansion curves in Figure 8 show the effects of the two different concentric regions of soil, as discussed previously where analytical results were validated against FE simulations. As the cavity size (a/a_0) is increased, the curves from the uniform soil tests reach a limit pressure. The limit pressure is reached quite quickly (in terms of a/a_0) for the uniform soil tests ($a/a_0 < 20$ for spherical and cylindrical tests), while the two-region tests reach the limit pressure after a much greater expansion (a/a_0 ranging from 250 to >500 for the spherical tests and from about 100 to 500 for the cylindrical tests).

The distinction between the two-region effects in the spherical and cylindrical analyses mentioned in discussion of Figure 5 can be explained using Figure 8. For the analysis, in which $a/a_0 = 60$, Figure 8 shows that the cavity pressure is generally dominated by the stiffness of Soil B, except for the spherical test 'CEM-1-10'. The two concentric zones have a significant effect in this spherical expansion test at the considered expansion state, whereas in the cylindrical analysis, the effect is minimal. This explains the difference in stress distributions between the spherical and cylindrical tests in Figure 5.

In Figure 9, the development of normalised plastic radius (c_A/a, c_B/a) in Soils A and B as the normalised cavity radius increases is presented for the case of spherical cavity expansion, as well as
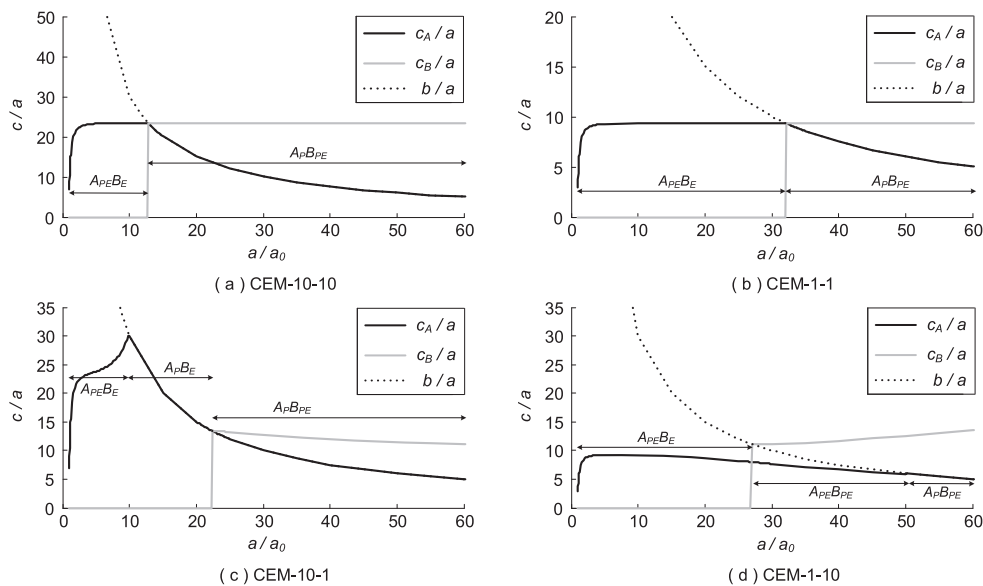
Figure 9. Development of plastic radii (c_A, c_B) in spherical tests: (a) CEM-10-10; (b) CEM-1-1; (c) CEM-10-1; (d) CEM-1-10.

the Soil A/B interface b/a, plotted with dotted lines. The uniform soil test results in Figure 9(a and b) show that plastic radius increases linearly with expansion after a small initial stage of nonlinear development ($a/a_0 < 5$). The growth of the plastic region is noted to be much faster in the test with higher stiffness, resulting in Soil A becoming fully plastic (A_P) at a much lower expansion ratio in test '10-10' ($a/a_0 = 12$) compared to test '-1-1' ($a/a_0 = 32$). For the two-region tests '-10-1' and '-1-10', the results in Figure 9(c and d) show the development of plastic radius within the different expansion stages (refer to Figure 2 for definition of labels). In test '-10-1', for a/a_0 between 11 and 22, Soil A is fully plastic while Soil B remains fully elastic ($A_P B_E$). In test '-1-10', there is a stage during which Soil B becomes partially plastic prior to Soil A becoming fully plastic ($A_{PE} B_{PE}$). The nonlinear behaviour of the plastic radius in the two-region tests is much more obvious compared to the uniform soil tests. All tests eventually tend towards an ultimate state in which further expansion generates a linear increase of the plastic radius (i.e. c_B/a levels off, which is discernible in the figures).

Figure 10 shows the equivalent results for the cylindrical cavity expansion. The cylindrical results show a significantly faster development (in terms of a/a_0) and higher value of plastic radius (c_A, c_B) compared to the spherical analysis results.

The spherical test 'CEM-1-10' is selected to study the effect of the variation of friction angle on the pressure–expansion curves and the development of cavity radius in Figure 11. The effect of the two different concentric regions of soil on cavity pressure (Figure 11(a)) is clearly shown where cavity pressure is initially controlled by Soil A but is then controlled by Soil B at larger expansion ratios. Plastic radius of Soil A (c_A) is dominated by Soil A ('$\phi_1 = 40\,°$; $\phi_2 = 40\,°$' is close to '$\phi_1 = 40\,°$; $\phi_2 = 20\,°$', and '$\phi_1 = 20\,°$; $\phi_2 = 20\,°$' overlaps '$\phi_1 = 20\,°$; $\phi_2 = 40\,°$'), as shown in Figure 11(b). The tests with a lower friction angle in Soil A have larger values of c_A, earlier appearance of c_B, and larger values of c_B. Figure 12 shows similar results for the effect of variation of dilation angle from spherical test 'CEM-1-10'. The development of plastic radius c_A and c_B are mainly controlled by Soil A, while a lower dilation angle in Soil A leads to a smaller value of c_A before Soil A becomes fully plastic (A_P).

The results of the two-region analyses also depend to a large degree on the size of Soil A. Indeed, for some critical size of Soil A, Soil B should have no effect on the results of the analysis. Figure 13 shows the variation of cavity pressure with the size of Soil A (given by b_0) for cavities expanded from $a_0 = 0.1$ mm to $a = 6$ mm. The results for the uniform soil tests are, as expected, unaffected by the variation of b_0. For the two-region tests, when b_0 is small, the cavity pressure is close to the uniform
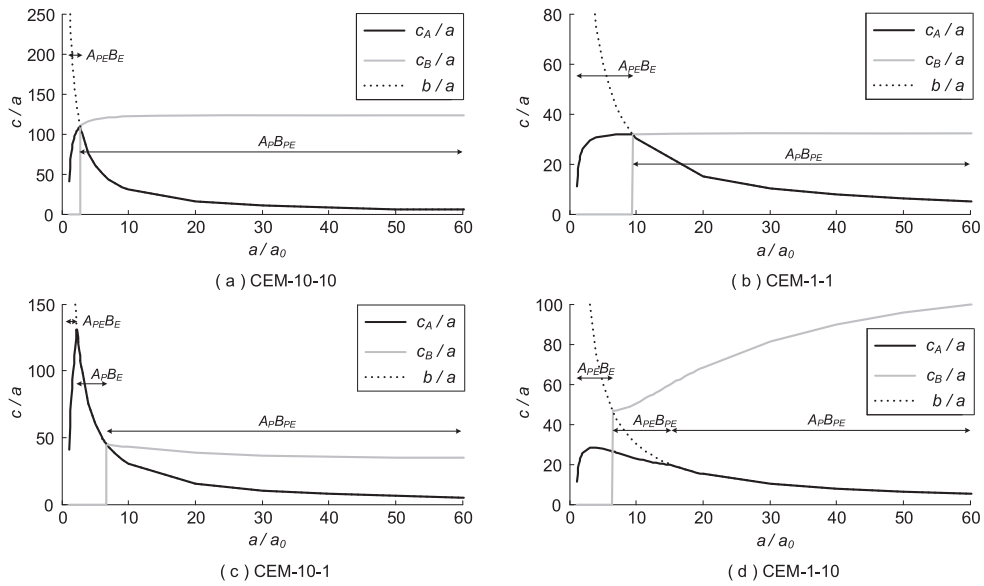
Figure 10. Development of plastic radii (c_A, c_B) in cylindrical tests: (a) CEM-10-10; (b) CEM-1-1; (c) CEM-10-1; (d) CEM-1-10.
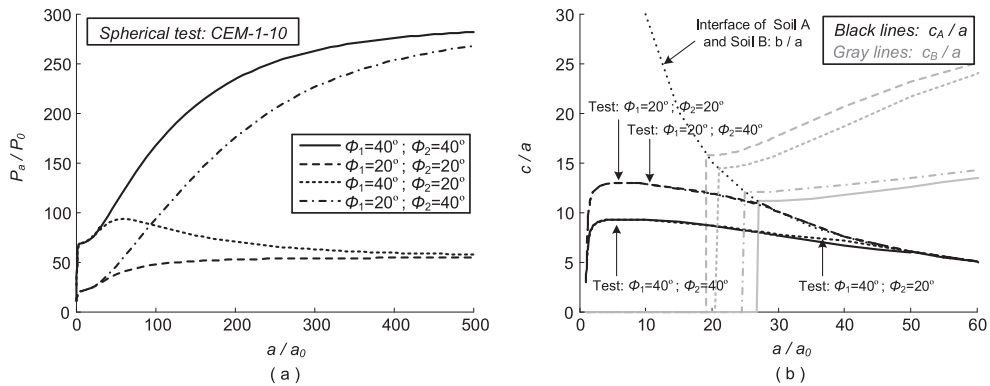

Figure 11. Developments of (a) cavity pressure and (b) plastic radii (c_A, c_B) with variation of friction angle for spherical test: CEM-1-10 (for $\psi_1 = \psi_2 = 10°$).
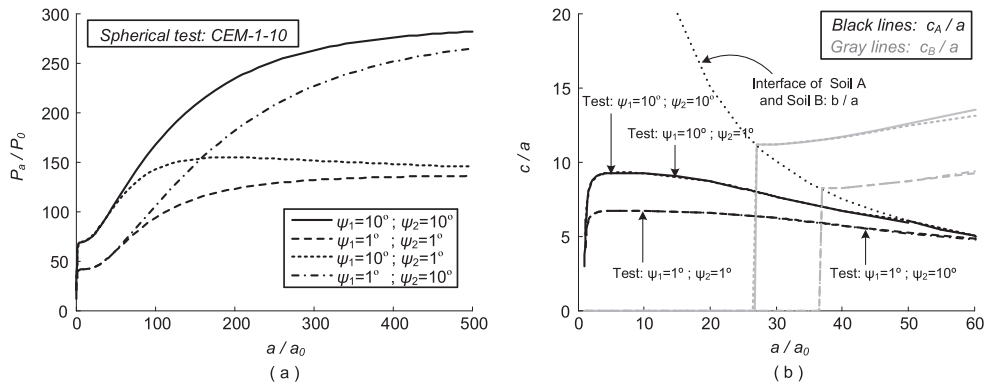

Figure 12. Developments of (a) cavity pressure and (b) plastic radii (c_A, c_B) with variation of dilation angle for spherical test: CEM-1-10 (for $\phi_1 = \phi_2 = 40°$).
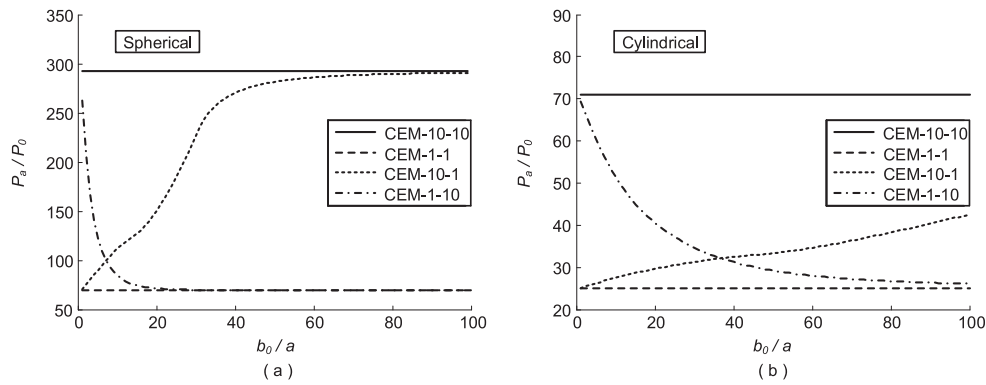
Figure 13. Variation of cavity pressure with size of Soil A (b_0): (a) spherical cavity expansion; (b) cylindrical cavity expansion.
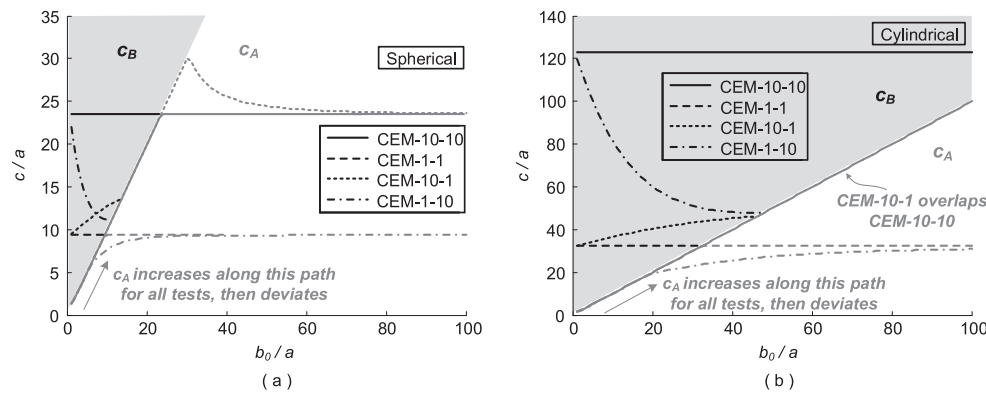

Figure 14. Variation of plastic radius (c_A, c_B) with thickness of Soil A (b_0): (a) spherical cavity expansion; (b) cylindrical cavity expansion.

soil test where E matches the value of E in Soil B of the two-region test. As b_0 increases, the two-region effects diminish, and the cavity pressure approaches the uniform soil test pressure in which E matches the value of E in Soil A of the two-region test. The value of b_0 at this stage can be considered as defining the critical size of Soil A, referred to as $b_{0,crit}$; for Soil A larger than $b_{0,crit}$, there will be no effect of the outer region of soil. For example, for the spherical test '-1-10' in Figure 13(a), the cavity pressure decreases from about 290 kPa (equivalent to the '-10-10' test) and approaches the pressure of the '-1-1' test when b_0/a is about 25. This value of b_0/a defines the critical size of Soil A in order for the two regions to have an effect in the spherical cavity expansion analysis. In contrast, the critical size for test '-10-1' is about three times larger than that of test '-1-10' ($b_0/a \cong 90$ where '-1-10' line approaches '-10-10' line), illustrating the effect of soil stiffness on the critical size. The cylindrical analysis results in Figure 13(b) show a much larger critical size compared to the spherical results.

Figure 14 shows the variation of plastic radius (c_A, c_B) with b_0 for both spherical and cylindrical analyses for cavity expansion from $a_0 = 0.1$ mm to $a = 6$ mm. The grey areas indicate values of the plastic radius in Soil B (c_B). The right-side boundary of the shaded area defines a line describing the linear increase of c_A with b_0 for all tests. The value of c_A eventually deviates from this line for all tests. Outside of the shaded area, c_B does not exist; the size of Soil A (defined by b_0) is great enough that plasticity does not commence within Soil B.

As expected, for the uniform soil tests, the plastic radius is unaffected by the variation of b_0. Considering the spherical test '-10-1' in Figure 14(a), c_B increases initially with b_0, although at a lower rate than c_A. The plastic region in Soil B disappears when $b_0/a \cong 15$ (where the '10-1' line for c_B meets the right-side boundary of the shaded area). Soil A is fully plastic until $b_0/a \cong 30$, after

which the value of c_A decreases towards and finally reaches the value obtained from the '-10-10' test at $b_0/a \cong 90$ (as the effects of Soil B gradually dissipate). In test '-1-10', c_B decreases initially with b_0 and c_A gradually increases and reaches the value from test '-1-1' at $b_0/a \cong 90$. This again defines the critical size of Soil A ($b_{0,crit}$) for the spherical analysis with the assumed material parameters. The cylindrical results in Figure 14(b) show similar trends to the spherical test.

6. COMMENTS ON GEOTECHNICAL APPLICATIONS

The results presented illustrate that the cavity expansion method can be effectively used to study problems involving two concentric regions of different soils. In reality, there are few geotechnical problems in which a true concentric condition exists. However, in some scenarios, the concentric assumption may prove to be of limited consequence to the application of the method to the more typical case of horizontally layered soils. The application of the method to the interpretation of CPT tip resistance or pile end bearing capacity in layered soils will be explored in future publications. The method may also have application to tunnelling and mining applications; however, the derivations would need to be modified for cavity contraction rather than expansion for these cases. Notably, the concentric assumption is directly applicable to the analysis of shaft construction using ground-freezing techniques, where a cylinder of frozen ground is surrounded by a zone of less stiff and weaker un-frozen ground.

7. CONCLUSIONS

An analytical solution for spherical and cylindrical cavity expansion in two different concentric regions of soil was presented and validated against FE simulations. The closed-form solutions are an extension of the cavity expansion solutions developed by Yu and Houlsby [4] and provide the stress and strain distributions within the two soils for both elastic and plastic states using a Mohr–Coulomb yield criterion, a non-associated flow rule, and a large-strain analysis. The effects of the two different concentric regions of soil were investigated by using pressure expansion curves and by studying the development of the plastic radius in both soil regions (c_A and c_B). The effect of variation of stiffness, strength, and plastic-flow parameters of both soils was illustrated, and the results highlighted the capability of the analytical solution. Despite the limitation of constant material properties, the proposed solution is potentially useful for various geotechnical problems involving aspects of soil layering, such as the interpretation of cone penetration test data, tunnelling and mining, and analysis of shaft construction using ground-freezing methods.

LIST OF NOTATION

a_0, a	radii of the cavity
b_0, b	radii of the Soil A/B interface
c_{0A}, c_A	radii of the plastic boundary in Soil A
c_{0B}, c_B	radii of the plastic boundary in Soil B
P_0	initial cavity pressure and in-situ hydrostatic stress
P_a	cavity pressure
P_b	radial stress at the boundary of two soil regions
P_{c_A}	radial stress at the plastic boundary of Soil A
P_{c_B}	radial stress at the plastic boundary of Soil B
E_1, E_2	Young's moduli for two soil regions
G_1, G_2	shear moduli for two soil regions
C_1, C_2	cohesions for two soil regions
ϕ_1, ϕ_2	friction angles for two soil regions
ψ_1, ψ_2	dilation angles for two soil regions
ν_1, ν_2	Poisson's ratios for two soil regions
M_1, M_2	functions of material properties for two soil regions
Y_1, Y_2	functions of material properties for two soil regions

α_1, α_2	functions of material properties for two soil regions
β_1, β_2	functions of material properties for two soil regions
γ_1, γ_2	functions of material properties for two soil regions
δ_1, δ_2	functions of material properties for two soil regions
μ_1, μ_2	functions of material properties for two soil regions
χ_1, χ_2	functions of material properties for two soil regions
σ_r, σ_θ	radial and tangential stresses, respectively
$\epsilon_r, \epsilon_\theta$	radial and tangential strains, respectively
u	radial displacement
D_1, D_2	constants of integration
A_1, A_2	constants of integration
Λ_1, Λ_2	infinite power series
R_2	cavity pressure ratio in Soil B
ϱ	auxiliary variable
n	integer from zero to infinity
D	radius of Soil B in Finite element models
r_0, r	radial positions of soil element in the model
k	parameter to combine cylindrical ($k = 1$) and spherical ($k = 2$) analysis
ϕ_{max}	peak friction angle
ϕ_{cs}	critical state friction angle
$b_{0,crit}$	critical size of Soil A

APPENDIX

The functions provided by Yu and Houlsby [6] for mathematical convenience are reproduced in what follows using the notation adopted in this paper. These equations apply separately to Soils A and B.

$$G = \frac{E}{2(1+v)} \qquad M = \frac{E}{1-v^2(2-k)} \qquad Y = \frac{2C\cos\phi}{1-\sin\phi} \qquad \alpha = \frac{1+\sin\phi}{1-\sin\phi}$$

$$\beta = \frac{1+\sin\psi}{1-\sin\psi} \qquad \gamma = \frac{\alpha(\beta+k)}{k(\alpha-1)\beta} \qquad \delta = \frac{Y+(\alpha-1)P_0}{2(\alpha+k)G}$$

REFERENCES

1. Gibson R, Anderson W. In situ measurement of soil properties with the pressuremeter. *Civil Engineering and Public Works Review* 1961; **56**(658):615–618.
2. Vesic AS. Expansion of cavities in infinite soil mass. *ASCE Journal of Soil Mechanics and Foundations Division* 1972; **98**(SM3):265–290.
3. Carter JP, Booker JR, Yeung SK. Cavity expansion in cohesive frictional soils. *Géotechnique* 1986; **36**(3):349–358.
4. Yu HS, Houlsby GT. Finite cavity expansion in dilatant soils: loading analysis. *Géotechnique* 1991; **41**(2):173–183.
5. Salgado R, Mitchell JK, Jamiolkowski M. Cavity expansion and penetration resistance in sand. *Journal of Geotechnical and Geoenvironmental Engineering* 1997; **123**(4):344–354.
6. Yu HS. *Cavity Expansion Methods in Geomechanics*. Kluwer Academic Publishers: the Netherlands, 2000.
7. Wroth CP. Interpretation of in situ soil tests. *Géotechnique* 1984; **34**(4):449–489.
8. Clarke BG. *Pressuremeter in Geotechnical Design*. Chapman and Hall: London, 1995.
9. Lunne T, Robertson PK, Powell JJM. *Cone Penetration Testing in Geotechnical Practice*. Blackie Academic and Professional: London, 1997.
10. Yu HS, Mitchell JK. Analysis of cone resistance: review of methods. *Journal of Geotechnical and Geoenvironmental Engineering* 1998; **124**(2):140–149.
11. Salgado R, Prezzi M. Computation of cavity expansion pressure and penetration resistance in sands. *International Journal of Geomechanics* 2007; **7**(4):251–265.
12. Davis RO, Scott RF, Mullenger G. Rapid expansion of a cylindrical cavity in a rate-type soil. *International Journal for Numerical and Analytical Methods in Geomechanics* 1984; **8**(2):125–140.
13. Randolph MF, Dolwin J, Beck R. Design of driven piles in sand. *Géotechnique* 1994; **44**(3):427–448.

14. Yasufuku N, Hyde AFL. Pile end-bearing capacity in crushable sands. *Géotechnique* 1995; **45**(4):663–676.
15. Collins IF, Yu HS. Undrained cavity expansions in critical state soils. *International Journal for Numerical and Analytical Methods in Geomechanics* 1996; **20**(7):489–516.
16. Hoek E, Brown ET. *Underground Excavations in Rock*. The Institution of Mining and Metallurgy: London, 1980.
17. Mair RJ, Taylor RN. Prediction of clay behaviour around tunnels using plasticity solutions. *Predictive Soil Mechanics – Proceedings of the Wroth Memorial Symposium*, Thomas Telford, London, 1993; 449–463.
18. Yu HS, Rowe RK. Plasticity solutions for soil behaviour around contracting cavities and tunnels. *International Journal for Numerical and Analytical Methods in Geomechanics* 1999; **23**(12):1245–1279.
19. Marshall AM. Tunnel-pile interaction analysis using cavity expansion methods. *ASCE Journal of Geotechnical and Geoenvironmental Engineering* 2012; **138**(10):1237–1246.
20. Marshall AM. Closure to "Tunnel-pile interaction analysis using cavity expansion methods" by Alec M. Marshall. *ASCE Journal of Geotechnical and Geoenvironmental Engineering* 2013; **139**(11):2002–2004.
21. Xu X, Lehane BM. Pile and penetrometer end bearing resistance in two-layered soil profiles. *Géotechnique* 2008; **58**(3):187–197.
22. Bernard RS, Hanagud SV. Development of a projectile penetration theory. report 1:penetration theory for shallow to moderate depths. *Technical Report*, U.S. Army Engineering Waterways Experiment Station, 1975.
23. Bernard RS. Development of a projectile penetration theory. Report 2: Deep penetration theory for homogeneous and layered targets. *Technical Report*, U.S. Army Engineering Waterways Experiment Station, 1976.
24. Sayed SM, Hamed MA. Expansion of cavities in layered elastic system. *International Journal for Numerical and Analytical Methods in Geomechanics* 1987; **11**(2):203–213.
25. Davis EH. Theories of plasticity and the failure of soil masses. In *Soil Mechanics*, Lee I (ed.). Butterworths: London, 1968.
26. Verruijt A, Booker JR. Surface settlements due to deformation of a tunnel in an elastic half plane. *Géotechnique* 1996; **46**(4):753–756.